

High Temperature Behavior of the Chern-Simons Diffusion Rate in the 1+1 D Abelian Higgs Model

Wai Hung Tang* and Jan Smit†

Institute of Theoretical Physics, University of Amsterdam
Valckenierstraat 65, 1018 XE Amsterdam, the Netherlands

June 19, 2018

Abstract

We give arguments that in the 1+1 dimensional abelian Higgs model the classical approximation can be good for the leading high temperature behavior of real time processes. The Chern-Simons diffusion rate (‘sphaleron rate’) is studied numerically in this approximation. New results at high temperature show a $T^{2/3}$ behavior of the rate at sufficiently small lattice spacing.

PACS numbers: 11.15.Ha, 11.15.Kc

Keywords: sphaleron, baryon number violation, abelian-Higgs model

*email: tang@phys.uva.nl

†email: jsmit@phys.uva.nl

1 Introduction

In theories of baryogenesis the rate of sphaleron transitions plays an important role [1, 2]. This rate is hard to calculate analytically, especially at high temperatures. Numerical simulations in the quantum theory have to face the problem of a complex ‘Boltzmann factor’ associated with real time correlation functions at finite temperature. For this reason a classical approximation was proposed some time ago [3], which has been tested in the abelian Higgs model in 1+1 dimensions [4–9]. At low temperatures the rate was found [4, 7, 6] to agree with a semiclassical analytical calculation [10], while at high temperatures the results have been somewhat confusing: ref. [8] argued for a $T^{2/3}$ behavior, while we argued [9] for T^2 behavior. We found in fact T^2 behavior at nonzero lattice spacing which turned into T -independence in the limit of zero lattice spacing. In the mean time simulations of the physically relevant SU(2) models in 3+1 dimensions have been improving [11–16] and the understanding of the classical approximation has been steadily increasing [17–24]. It therefore appropriate to return to the abelian Higgs model and try to assess the situation in 1+1 dimensions. We give a more full account of our earlier work briefly reported in [9].

In sect. 2 we introduce the model and the rate of fermion number violation and we discuss some of their properties. The classical approximation is introduced in sect. 3 and studied in perturbation theory. Sect. 4 and 5 give details on the numerical method, sects. 6 and 7 contain results on the rate in the regimes of low and high temperatures and sect. 8 contains our conclusions. Details on the simulation algorithm using ‘Kramers equation’ are in the appendix.

2 Abelian-Higgs model

The classical abelian-Higgs model is given by the action

$$S = - \int d^2x \left[\frac{1}{4g^2} F_{\mu\nu} F^{\mu\nu} + (D_\mu \phi)^* D^\mu \phi + \mu^2 |\phi|^2 + \lambda |\phi|^4 \right], \quad (1)$$

with $F_{\mu\nu} = \partial_\mu A_\nu - \partial_\nu A_\mu$ and $D_\mu \phi = (\partial_\mu - iA_\mu)\phi$ (our metric is given by $g_{00} = -g_{11} = -1$). We recall that A_μ , $\sqrt{\lambda}$ and g have dimension of mass, while ϕ is dimensionless in 1+1 dimensions. The role of a dimensionless coupling is played by $\lambda/|\mu^2|$, at given $\xi = g^2/\lambda$.

The classical model has a Higgs phase for $\mu^2 < 0$, where ϕ gets a ground state expectation value $|\phi| = v/\sqrt{2}$, $v^2 = -\mu^2/\lambda$, with masses $m_\phi^2 = 2\lambda v^2$, $m_A^2 = g^2 v^2$. In the euclidean version of the quantum theory there is a Berezinsky-Kosterlitz-Thouless phase transition in the scalar model at $g = 0$ which is turned into a crossover at nonzero gauge coupling [25, 26]. For a recent lattice study, see [27]. At nonzero temperature there is only a crossover in any case because then the system is infinite in one dimension only.

A toy model for the electroweak theory is obtained by coupling to fermions,

$$S_F = - \int d^2x \left[\bar{\psi} \gamma^\mu (\partial_\mu + i \frac{1}{2} A_\mu \gamma_5) \psi + y \bar{\psi} (\phi P_R + \phi^* P_L) \psi \right] , \quad (2)$$

where $P_{L,R} = (1 \mp \gamma_5)/2$ are the chiral projectors. In the quantum theory the fermion current is anomalous,

$$\partial_\mu \bar{\psi} i \gamma^\mu \psi = -q , \quad (3)$$

with q the topological charge density ($\epsilon_{01} = +1$)

$$q = \frac{1}{4\pi} \epsilon^{\mu\nu} F_{\mu\nu} = \partial_\mu C^\mu , \quad (4)$$

where C^μ the Chern-Simons current

$$C^\mu = \frac{1}{2\pi} \epsilon^{\mu\nu} A_\nu . \quad (5)$$

As a consequence a change in Chern-Simons number

$$C = \int_0^L dx C^0 = -\frac{1}{2\pi} \int_0^L dx A_1 \quad (6)$$

is accompanied by a change in fermion number

$$F = \int_0^L dx \bar{\psi} i \gamma^0 \psi , \quad (7)$$

such that

$$F(t) - F(0) = -[C(t) - C(0)] = - \int_0^t dt' \int_0^L dx q(x, t') . \quad (8)$$

We take space to be a circle with circumference L .

The sphaleron rate Γ can be identified from the diffusion of Chern-Simons number [28],

$$\Gamma = \frac{1}{t} \langle [C(t) - C(0)]^2 \rangle, \quad t \rightarrow \infty. \quad (9)$$

In the following we shall neglect the influence of the fermions on the Bose fields. Our task is to evaluate the above real time correlation function.

Transitions with ΔC of order 1 have to cope with the sphaleron barrier of energy $E_s = (2/3)v^2 m_\phi$, for which $C = 1/2$ [29]. The sphaleron configuration can be written in the form

$$A_0 = 0, \quad A_1 = \frac{\pi}{L}, \quad \phi = \frac{v}{\sqrt{2}} \tanh\left(\frac{m_\phi}{2} y\right) \exp\left(i\frac{\pi}{L} y - i\frac{\pi}{2}\right),$$

where $y = x - L/2 \in (-L/2, L/2)$. At relatively low temperatures $m_\phi^2 \ll T \ll E_s$ the rate has been calculated semiclassically with the result [10]

$$F \equiv \frac{\Gamma}{m_\phi^2 L} = f(\xi) \sqrt{\frac{E_s}{T}} e^{-E_s/T}, \quad (10)$$

$$f(\xi) = \left[\frac{3}{(2\pi)^3} (s+1) \frac{\Gamma(\alpha+s+1)\Gamma(\alpha-s)}{\Gamma(\alpha+1)\Gamma(\alpha)} \right]^{1/2}, \quad (11)$$

$$\alpha = \sqrt{2\xi}, \quad s = \frac{1}{2} \left(-1 + \sqrt{1+8\xi} \right). \quad (12)$$

At high temperatures the rate is difficult to calculate analytically. On dimensional grounds it seems reasonable to expect that for temperatures T larger than any mass scale, in particular $T \gg E_s$,

$$\frac{\Gamma}{L} = \kappa(\xi) (v^{-2} T)^2, \quad (13)$$

with dimensionless κ . This formula is analogous to dimensional $\Gamma/L^3 = \kappa(\alpha_W T)^4$ in 3+1 dimensions, with v^{-2} playing the role of the electroweak coupling α_W . However, the behavior (13) is not obvious, since the original couplings λ and g^2 are dimensionful. At high temperature the dimensional reduction approximation leads to temperature appearing in the combinations λT and $g^2 T$. Since these have engineering dimension three in mass units, we may expect the behavior

$$\frac{\Gamma}{L} = \tilde{\kappa}(\xi) (\lambda T)^{2/3}, \quad (14)$$

instead of (13).

3 Classical approximation

The rate Γ defined by (9) is a nonperturbative quantity and one approach to its computation is by numerical simulation. This is well-known to be difficult since the effective Boltzmann factor in real time processes is complex:

$$\langle [C(t) - C(0)]^2 \rangle = \frac{\text{Tr} e^{-H/T} [e^{iHt} C(0) e^{-iHt} - C(0)]^2}{\text{Tr} e^{-H/T}}. \quad (15)$$

To cope with the complex weights a classical approximation has been introduced [3, 4] in which the quantum mechanical expectation value (15) is replaced by a classical expression,

$$\langle [C(t) - C(0)]^2 \rangle = \frac{\int D\varphi D\pi e^{-H_{\text{eff}}(\varphi,\pi)/T} [C(\varphi(t), \pi(t)) - C(\varphi, \pi)]^2}{\int D\varphi D\pi e^{-H_{\text{eff}}(\varphi,\pi)/T}}. \quad (16)$$

Here φ and π denote generic canonical variables and $\varphi(t)$ and $\pi(t)$ are solutions of the classical Hamilton equations with an effective hamiltonian H_{eff} and initial conditions $\varphi(0) = \varphi$, $\pi(0) = \pi$. This approximation is used at high temperature, where the important low momentum modes have high occupation numbers.

The classical approximation has been studied in perturbation theory in 3+1 dimensions [17–21]. For static quantities the situation is well understood, as this corresponds to dimensional reduction in the imaginary time formalism, of a 4D theory to a 3D theory which can be renormalized in the usual way. For time dependent quantities there are divergent effects in classical gauge theories (related to the physics of Landau damping) which are non-local and cannot be absorbed by local counterterms. In the renormalizable quantum theory such effects correspond to loop momenta of order of the temperature – the well known hard thermal loop effects.

In 1+1 dimensions the UV-divergencies are less severe. We shall now study the classical approximation for the abelian Higgs model in perturbation theory, using the imaginary time formalism and making an analytic continuation to real time at a suitable point. For simplicity we choose the classically symmetric phase $\mu^2 > 0$ for the starting point of perturbation theory. As a consequence the bare A -mass is zero, which causes infrared divergences in the diagrams. Such infrared divergences are presumably an artefact of perturbation theory and we assume they are cured automatically in a correct nonperturbative treatment. Here we shall use brute force and

introduce an infrared regulator mass m_A . This crude method breaks gauge invariance but it is adequate for our purpose of elucidating the classical approximation.

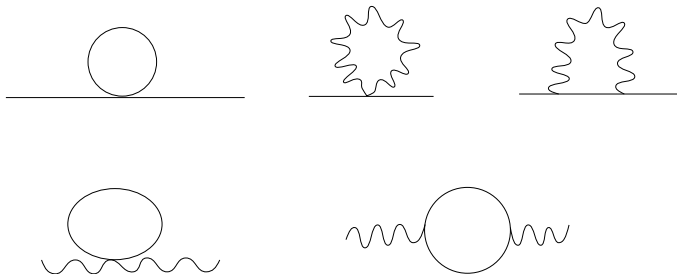


Figure 1: Higgs and gauge field selfenergy diagrams.

Consider the gauge boson contribution to the ϕ selfenergy given by the appropriate diagrams in Fig. 1:

$$\Sigma(p) = g^2 T \sum_n \int_{\mathbf{k}} \left[\delta_{\mu\nu} - \frac{(k+2p)_\mu (k+2p)_\nu}{m_\phi^2 + (k+p)^2} \right] D_{\mu\nu}(k), \quad (17)$$

$$\int_{\mathbf{k}} \equiv \int \frac{d^{D-1}k}{(2\pi)^{D-1}}, \quad (18)$$

where D ($\rightarrow 2$) is the number of spacetime dimensions, $k_D = n2\pi T$ are the Matsubara frequencies ($n = 0, \pm 1, \pm 2, \dots$), and the vector propagator is given by

$$D_{\mu\nu}(k) = \left[\delta_{\mu\nu} + (\alpha - 1) \frac{k_\mu k_\nu}{k^2} \right] \frac{1}{m_A^2 + k^2}. \quad (19)$$

For illustration we first choose the Feynman gauge $\alpha = 1$ and follow a standard method [30], which consists of carrying out the sum over Matsubara modes in the loop diagrams and subsequently analytically continuing the time component p_D of the external momentum to real frequencies p^0 . Writing $(k+2p)^2 = 2[m_\phi^2 + (k+p)^2] - [m_A^2 + k^2] - (2m_\phi^2 - m_A^2 - 2p^2)$, to conveniently cancel the time component of the loop momentum in the numerator against the denominators, we get

$$\begin{aligned} \Sigma = g^2 \int_{\mathbf{k}} & \left\{ (D-2) \frac{1+2n}{2\omega} + \frac{1+2n'}{2\omega'} + \frac{2m_\phi^2 - m_A^2 - 2\mathbf{p}^2 + 2p_0^2}{2\omega\omega'} \right. \\ & \left. \times \left[\frac{(1+n+n')(\omega+\omega')}{(\omega+\omega')^2 - p_0^2} - \frac{(n-n')(\omega-\omega')}{(\omega-\omega')^2 - p_0^2} \right] \right\}, \end{aligned} \quad (20)$$

where

$$\begin{aligned} n &= \frac{1}{e^{\omega/T} - 1}, & n' &= \frac{1}{e^{\omega'/T} - 1}, \\ \omega &= \sqrt{m_A^2 + \mathbf{k}^2}, & \omega' &= \sqrt{m_\phi^2 + (\mathbf{k} + \mathbf{p})^2}. \end{aligned} \quad (21)$$

The external real-time frequency $p^0 = -p_0$ is supposed to have a small positive imaginary part, $p^0 \rightarrow p^0 + i\epsilon$, which corresponds to retarded boundary conditions.

The zero temperature contribution, obtained by letting $n, n' \rightarrow 0$, has a logarithmic UV-divergence which can be canceled by a mass counterterm. The temperature dependent contribution is finite as usual. We now add the mass counterterm to Σ , assume dimensional renormalization in the MS-bar scheme, and denote the resulting selfenergy by $\bar{\Sigma}$. We are interested in its high temperature behavior when $T \gg m_A, m_\phi, |\mathbf{p}|, p^0$.

For high temperatures it turns out that the leading contribution in a high temperature expansion is obtained by substituting the leading behavior of the Bose distribution functions n and n' ,

$$\frac{1}{2} + n \rightarrow \frac{T}{\omega}, \quad \frac{1}{2} + n' \rightarrow \frac{T}{\omega'}. \quad (22)$$

The resulting expression can be written as

$$\begin{aligned} \Sigma_c &= g^2 T \int_{\mathbf{k}} \left\{ \frac{D-2}{\omega^2} + \frac{1}{\omega'^2} + \frac{2m_\phi^2 - m_A^2 - 2\mathbf{p}^2 + 2p_0^2}{2\omega^2\omega'^2} \right. \\ &\quad \left. \times \left[\frac{(\omega + \omega')^2}{(\omega + \omega')^2 - p_0^2} + \frac{(\omega - \omega')^2}{(\omega - \omega')^2 - p_0^2} \right] \right\}. \end{aligned} \quad (23)$$

This is finite for $D = 2$, which justifies the replacement (22) under the integral. This contribution is actually identical to the classical selfenergy which follows from (16), hence the subscript c . Intuitively this is plausible, since large occupation numbers n, n' imply classical behavior, although it is of course not obvious that solving the classical equations of motion and averaging over initial conditions according to (16) leads to the same correlation functions as making the high temperature approximation (22). See [20] for more details in scalar field theory.

For $p^0 = 0$ the classical selfenergy Σ_c goes over into the selfenergy of the naively dimensionally reduced theory, the one dimensional field theory

obtained by keeping only the zero mode ($n = 0$) in (17). In this case Σ is the selfenergy of the zero mode $\int_0^{1/T} dx_D \phi(\mathbf{x}, x_D)$.

The difference between the classical and quantum selfenergy is subleading for large T and it can be expressed as

$$\begin{aligned}\bar{\Sigma} - \Sigma_c &= \frac{g^2}{2\pi} \left(c - \ln \frac{T}{\bar{\nu}} \right) + O(T^{-1}), \\ c &= -\ln 2 - 1 + \int_0^\infty dx \left[\left(1 + \frac{2}{e^x - 1} - \frac{2}{x} \right) \frac{1}{x} - \frac{1}{(1+x)} \right],\end{aligned}\tag{24}$$

where $\bar{\nu}$ is the scale parameter in the MS-bar scheme. We have subtracted and added the logarithmic UV-divergence in the form $\int_{\mathbf{x}} (1 + |\mathbf{x}|)^{-1}$. The momentum dependence of $\bar{\Sigma} - \Sigma_c$ is in the $O(T^{-1})$ terms. Although $\bar{\Sigma} - \Sigma_c$ has been calculated in the Feynman gauge, its leading T contribution given by the first term in (24) is in fact independent of the gauge parameter α . This can be seen by going back to (17), setting $p = 0$ and subtracting the $n = 0$ mode. We can easily add the contribution of the $\lambda(\phi^*\phi)^2$ interaction to the selfenergy. The complete one loop $\bar{\Sigma} - \Sigma_c$ is obtained by $g^2 \rightarrow g^2 + 4\lambda$ in (24).

Consider next the gauge field self energy tensor $\Pi_{\mu\nu}$ corresponding to the diagrams in Fig. 1,

$$\Pi_{\mu\nu}(p) = g^2 T \sum_n \int_{\mathbf{k}} \left[\frac{2\delta_{\mu\nu}}{m_\phi^2 + k^2} - \frac{(2k+p)_\mu(2k+p)_\nu}{m_\phi^2 + k^2)(m_\phi^2 + (k+p)^2)} \right].\tag{25}$$

The logarithmic divergence of each of the two contributing diagrams cancels in the sum, which can be shown by using the Ward-Takahashi identity $p_\mu \Pi_{\mu\nu}(p) = 0$. In 1+1 dimensions this identity furthermore tells us there is only one independent component in $\Pi_{\mu\nu}$, which we choose to be Π_{11} . Summing over the Matsubara frequencies and continuing p_2 analytically to p^0 we get

$$\begin{aligned}\Pi_{11} &= g^2 \int_{\mathbf{k}} \left\{ \frac{2(1+2n)}{2\omega} - \frac{(2k_1+p_1)^2}{2\omega\omega'} \right. \\ &\quad \left. \times \left[\frac{(1+n+n')(\omega+\omega')}{(\omega+\omega')^2 - p_0^2} - \frac{(n-n')(\omega-\omega')}{(\omega-\omega')^2 - p_0^2} \right] \right\},\end{aligned}\tag{26}$$

where now $\omega = \sqrt{m_\phi^2 + \mathbf{k}^2}$ (ω' , n and n' are as in (21)). The dominant large T behavior of Π_{11} is given by its classical approximation obtained with the

substitution (22),

$$\Pi_{11}^c = g^2 T \int_{\mathbf{k}} \left\{ \frac{2}{\omega^2} - \frac{(2k_1 + p_1)^2}{2\omega^2 \omega'^2} \left[\frac{(\omega + \omega')^2}{(\omega + \omega')^2 - p_0^2} + \frac{(\omega - \omega')^2}{(\omega - \omega')^2 - p_0^2} \right] \right\}, \quad (27)$$

which is UV-finite and of order T . The next to leading behavior turns out to be of order T^0 (not $\ln T$):

$$\Pi_{11} - \Pi_{11}^c = \frac{g^2}{\pi} \frac{p_0^2}{p_1^2 - p_0^2} + O(T^{-1}). \quad (28)$$

This contribution corresponds to loop momenta \mathbf{k} of order T and it is therefore the analogue of the hard thermal loop expression in 3+1 dimensions. Here in 1+1 dimensions it is subdominant to the classical Π_{11}^c . All other diagrams are superficially UV-convergent in two dimensions and for convergent diagrams the corrections to the approximation (22) are down by two powers T , as follows for example from the fact that they correspond to the $n \neq 0$ terms in the summation over Matsubara frequencies.

We conclude that in two dimensions the classical theory is a good approximation to the quantum theory, for weak coupling. The classical theory is UV-finite. To minimize the difference between the classical and quantum theory we can match the classical mass parameter μ_c^2 of the Higgs field according to

$$\mu_c^2 = \bar{\mu}^2 + \bar{\Sigma} - \Sigma_c = \bar{\mu}^2 + \frac{g^2 + 4\lambda}{2\pi} \left(c - \ln \frac{T}{\bar{\nu}} \right), \quad (29)$$

where the bar on the right hand side indicates the MS-bar scheme. However, this matching is only of limited use since we cannot match the corresponding non-analytic subdominant terms in $\Pi_{\mu\nu}$ with a local classical action.

An important point is now that we can take a limit of weak coupling and high temperature, such that the classical approximation becomes exact:

$$\lambda = v^{-2} |\bar{\mu}^2|, \quad g^2 = \xi \lambda, \quad T = v^2 |\bar{\mu}| T', \quad v^2 \rightarrow \infty. \quad (30)$$

The limit is such that T' and ξ are kept fixed. Note that $T' = \lambda T / |\bar{\mu}|^3$, and λT and $g^2 T$ are the combinations appearing in the dimensionally reduced theory. In this limit $\mu_c^2 / \bar{\mu}^2 \rightarrow 1$ and the quantum corrections (24) and (28) go to zero. In (30) we have written $|\mu|$ such that it also applies to the classical Higgs phase, for which $\mu^2 < 0$. Instead of $\bar{\mu}$ we can of course use any convenient mass scale, e.g. the zero temperature Higgs mass.

If we do not take the above limit, the question arises, how accurate is the classical approximation. The above calculations are carried out for external frequencies and momenta which are small compared to the temperature. On the other hand, in real time (as opposed to frequency space) we also may expect a limited region of validity. The correction (28) leads to propagation and situations might exist where it becomes substantial, depending on the physical quantity under study. In the application to the computation of the sphaleron rate, the Chern-Simons number is a zero momentum observable (explicitly so in Coulomb gauge), and the rate is should be dominated by low frequencies (cf. the cosine transform method in [14]).

The classical approximation is on a much better footing in 1+1 dimensions than in 3+1 dimensions, because it gives directly the dominant high temperature behavior of correlation functions, not only in the static case corresponding to dimensional reduction, but also in case of time dependence. (The classical partition function still suffers from the Rayleigh-Einstein-Jeans divergence.) In 4D, matching mass parameters between the original theory and the dimensionally reduced theory involves not only the classical combinations g^2T and λT , but also g^2T^2 and λT^2 . The latter combinations correspond to the well known hard thermal loops effects, which are the result of loop momenta of order of the temperature, and which reflect the quadratic divergences in the bare theory. Since g^2T^2 dominates over $g^2T|\bar{\mu}|$, the details of the matching formulas are important in four dimensions even in the weak coupling limit. In 2D, such matching can be ignored in the weak coupling limit (30).

4 Lattice regularization

The classical partition function is still a functional integral over all $\varphi(\mathbf{x})$ and $\pi(\mathbf{x})$ and needs regularization. In the numerical simulations this is provided by a lattice, for which the action takes the form.

$$\begin{aligned}
S = \int dt a \sum_{n=0}^{N-1} & \left\{ \frac{1}{2g^2} [(A_{0n+1} - A_{0n})/a - \partial_0 A_{1n}]^2 \right. \\
& + |(\partial_0 - iA_{0n})\phi_n|^2 - |\exp(-iaA_{1n})\phi_{n+1} - \phi_n|^2/a^2 \\
& \left. - \lambda \left[|\phi_n|^2 - \frac{v^2}{2} \right]^2 \right\}, \tag{31}
\end{aligned}$$

where a is the lattice distance, $L = Na$ and $v^2 = -\mu^2/\lambda$. From now on we only consider the case $\mu^2 < 0$. In the previous section we gave arguments that we can use this action in the classical approximation, provided we replace μ^2 by an effective parameter μ_c^2 which is related to $\bar{\mu}^2$ in the MS-bar scheme by (29). In the weak coupling-high temperature limit (30) the difference between μ_c^2 and $\bar{\mu}^2$ may be neglected, which is what we shall do in the following. Accordingly, we drop the subscript c on μ^2 and v^2 .

We use the Coulomb gauge to obtain a hamiltonian description. The gauge condition $A_{1n+1} - A_{1n} = 0$ states that A_1 is independent of n and related to the Chern-Simons number C by,

$$aA_1 = 2\pi C/N. \quad (32)$$

The Gauss constraint

$$\sum_n \Delta_{mn} A_n^0 \equiv A_{m+1}^0 + A_{m-1}^0 - 2A_m^0 = -a^2 g^2 j_m^0, \quad (33)$$

where $j^0 = -j_0$ is the charge density,

$$j_0 = -i\phi^* D_0 \phi + i(D_0 \phi)^* \phi, \quad (34)$$

is solved explicitly as

$$A_m^0 = -a^2 g^2 \sum_n \Delta_{mn}^{-1} j_n^0, \quad (35)$$

under conditions with zero total charge $Q = a \sum_n j_n^0$. The canonical momenta are defined by $\pi_n = \partial L / \partial \dot{\phi}_n$, etc. where $S = \int dt L$.

It will be convenient in the following to use $|\mu| = \sqrt{\lambda}v$ as the basic unit of mass and to use scaled quantities, indicated with a prime,

$$a = \frac{a'}{v\sqrt{\lambda}}, \quad t = \frac{t'}{v\sqrt{\lambda}}, \quad \phi = v\phi', \quad A_\mu = v\sqrt{\lambda}A'_\mu. \quad (36)$$

Then

$$\begin{aligned} S &= v^2 S', \\ S' &= \int dt' a' \sum_{n=0}^{N-1} \left\{ \frac{1}{2\xi} [(A'_{0n+1} - A'_{0n})/a' - \partial'_0 A'_{1n}]^2 \right. \\ &\quad + |(\partial'_0 - iA'_{0n})\phi'_n|^2 - |\exp(-ia'A'_{1n})\phi'_{n+1} - \phi'_n|^2 / a'^2 \\ &\quad \left. - \left[|\phi'_n|^2 - \frac{1}{2} \right]^2 \right\}, \end{aligned} \quad (38)$$

and the hamiltonian can be written as

$$H = v^3 \sqrt{\lambda} H', \quad (39)$$

$$H' = \frac{1}{2} \frac{\xi L'}{(2\pi)^2} P_C^2 + \sum_{n=0}^{N-1} \left\{ \frac{|\pi'_n|^2}{a'} + \frac{|\exp(-i2\pi C/N) \phi'_{n+1} - \phi'_n|^2}{a'} \right. \\ \left. + a' \left(|\phi'_n|^2 - \frac{1}{2} \right)^2 + \frac{a'^3 \xi}{2} \sum_{m,n=0}^{N-1} j_m'^0 \Delta_{mn}^{-1} j_n'^0 \right\}, \quad (40)$$

$$j_n'^0 = (-i\pi'_n \phi'_n + i\pi_n'^* \phi_n'^*) / a', \quad (41)$$

where P_C , π'_n and $\pi_n'^*$ are the canonical momenta conjugate to C , ϕ'_n and $\phi_n'^*$. The Poisson brackets are normalized to one, e.g. $\{\phi'_m, \pi'_n\} = \delta_{mn}$. The classical partition function is given by

$$Z = \int dP_C dC \prod_n (d\pi'_n d\pi_n'^* d\phi'_n d\phi_n'^*) \exp\left(-\frac{H'}{T'}\right) \quad (42)$$

with T' defined by

$$T = v^3 \sqrt{\lambda} T', \quad (43)$$

in accordance with (30). The C integration is over the compact domain $-N/2 \leq C \leq N/2 \pmod{N}$. We also define a scaled diffusion rate Γ' by

$$\Delta(t) \equiv \langle [C(t) - C(0)]^2 \rangle \rightarrow \Gamma t = \Gamma' t', \quad (44)$$

for large times.

It is easy to see that there are N classical ground states given by

$$C = k = 0, 1, \dots, N-1, \quad \phi' = \frac{1}{\sqrt{2}} \exp(i2\pi kn/N),$$

and $P_C = \pi'_n = 0$. Writing $\phi'_n = \rho_n \exp(i\theta_n)$ we can introduce a winding number of the scalar field by

$$w = \frac{1}{2\pi} \sum_{n=0}^{N-1} \partial\theta_n, \quad \partial\theta_n \equiv \theta_{n+1} - \theta_n \pmod{2\pi} \in (-\pi, \pi].$$

Then also $w = k$ in the ground states. Both C and w are defined modulo N .

For convenience we record various scaled quantities:

$$E_s = v^3 \sqrt{\lambda} E'_s, \quad m_\phi = v \sqrt{\lambda} m'_\phi, \quad m_A = v \sqrt{\lambda} m'_A, \quad (45)$$

$$E'_s = \frac{2\sqrt{2}}{3}, \quad m'_\phi = \sqrt{2}, \quad m'_A = \sqrt{\xi}, \quad (46)$$

which characterize the scaled theory given by the action S' or hamiltonian H' . We also have

$$\begin{aligned} F &= \frac{\Gamma}{m_\phi^2 L} = \frac{\Gamma'}{m_\phi'^2 L'} \\ &\rightarrow \frac{1}{2} \kappa T'^2 \quad \text{or} \quad \rightarrow \frac{1}{2} \tilde{\kappa} T'^{2/3}, \end{aligned} \quad (47)$$

for the large temperature behavior (13) or (14).

5 Numerical method

It is straightforward to derive Hamilton's equations from the Coulomb gauge hamiltonian (40). We use a second order Langevin procedure to generate initial conditions according to the canonical ensemble. In this procedure, also known as the Kramers equation method, Hamilton's equations are modified by adding noise and friction terms to the equations for the canonical momenta. If this is done straightforwardly local 'current conservation' $0 = \partial_0 j_n^0 + (j_{n+1}^1 - j_n^1)/a \sim \partial_\mu j^\mu$ would be violated, since j^0 contains the momentum of the scalar field. Consequently the total charge Q would be nonzero, which is a problem for the evaluation of the Coulomb energy. To deal with these constraints (which are similar to the Gauss constraint in the temporal gauge) we follow ref. [5] and use polar coordinates $\phi' = \rho \exp(i\theta)$. The random Langevin forces are then only applied to the gauge invariant variables ρ , p_ρ , and not to the gauge variant θ , p_θ . See the appendix for a description of the algorithm. The random forces are also not applied to C and P_C either, which makes it possible to monitor thermalization of P_C . In practice the singularity of the polar coordinates can lead to problems at the origin $\rho = 0$. We dealt with this in the following way. The system is kicked at time intervals $\Delta t' = h$ by the random forces. If the kick is large in some sense, the updated coordinates may get too close to the origin, causing large discretization errors. We avoid this by replacing the single step update

by a variable stepsize leapfrog algorithm for the integration of Hamilton's equations over the interval $(t', t' + h)$. The Langevin stepsize is still given by h , however.

The finite Langevin stepsize h introduces an error which we monitored by requiring the 'output temperatures' T'_C and T'_ρ ,

$$\left\langle \frac{\xi L P_C^2}{4\pi^2} \right\rangle = T'_C = \beta_C^{-1}, \quad \left\langle \frac{p_\rho^2}{2a} \right\rangle = T'_\rho = \beta_\rho^{-1}, \quad (48)$$

to be such that $\beta_{C,\rho}$ differed less than 0.1 in absolute value from $\beta \equiv 1/T'$. This criterion is based on the interpretation that small Langevin errors lead to an effective temperature, the output temperature. Then the expectation $\Gamma' \propto \exp(-\beta E'_s)$, with $E'_s = 2\sqrt{2}/3 \approx 0.94$ suggests that an absolute error in β of ≈ 0.1 , causes a relative error in Γ' of $\approx 10\%$.

Having produced an independent configuration of p 's and q 's we took this as the initial condition for the real time integration of Hamilton's equations. For this we could use the original cartesian coordinates, as the condition of charge zero is easily satisfied by projecting regularly onto zero charge (this only involves changes of machine precision order). After real time integration the Langevin process was started again and the process was repeated until sufficient statistics was obtained.

Our configurations were actually microcanonical to some extent, because the Langevin processes were stopped (for historical reasons) at times that the total energy had its mean value. As expected, we found in a few checks that the true canonical ensemble gave the same results within errors. The friction parameter was taken $f = 1$, and we checked that results do not depend on f , as should be the case.

An accurate fifth order Adams-Bashforth-Moulton predictor-corrector multi-step integration algorithm was used to keep the numerical drift in the total energy sufficiently small. Otherwise we found that the diffusion Δ turned out not to be linear in t' for large t' .

6 Low temperature region

The results that will be presented are for $\xi = g^2/\lambda = 4$, for which $m'_A = 2 = \sqrt{2}m'_\phi$. Fig. 2 shows the behavior of $\langle |\phi'|^2 \rangle$ as a function of β . We see a minimum near $\beta = 3$ where the crossover takes place between the low temperature region ($\beta > 3$) and the high temperature region ($\beta < 3$). Recall

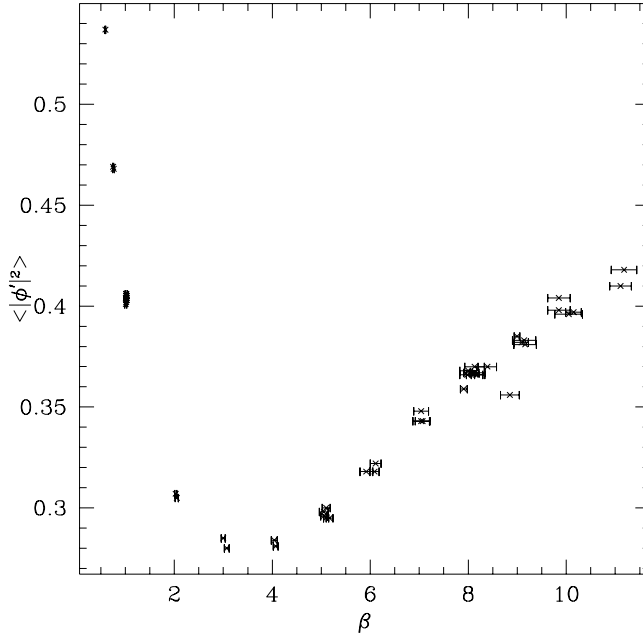


Figure 2: $\langle |\phi'|^2 \rangle$ versus β .

that even this ‘low temperature region’ can be interpreted as a region of high unscaled temperatures: $T/m_\phi = v^2/(\sqrt{2}\beta) \rightarrow \infty$ as $v^2 \rightarrow \infty$.

For low temperatures the Chern-Simons diffusion Δ tends to be small and large times t were needed to get $\Delta > 1$. For the evaluation of the rate we require $\Delta > 10$, such that at least three sphaleron transitions take place ($\Delta C \gtrsim 3$).

In fig. 3 a comparison is made with the analytic semiclassical result (12). The upper data are for $a' = 0.32$, the lower data for $a' = 0.16$ (at $\beta = 10, 11$ for $a' = 0.32$ only). The system size is $L' = 16$ ($N = 50$ and $N = 100$). We obtained the same results within errors for the smaller volume $L' = 10.28$, in a check for a few β values. However, for sizes as low as $L' = 8$ we did see clear deviations in the low temperature regime. The errors in the rate Γ are statistical and determined with the jackknife method from at least 900 configurations. For β we used the output temperature (48), with errors obtained by the binning method. The input β is the nearest integer.

We conclude from fig. 3 that the classical simulation is able to reproduce the semi-classical formula for $\beta \gtrsim 7$. For the two lattice spacings $a' = 0.32$,

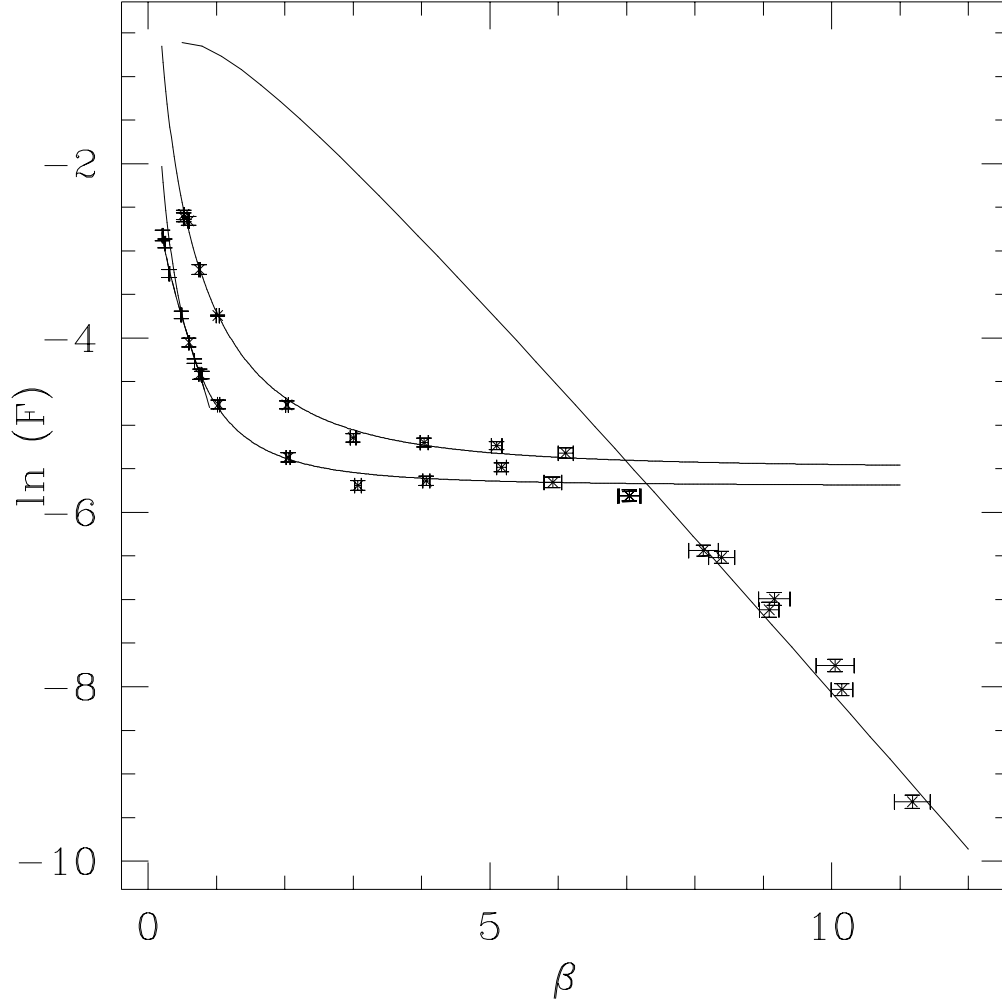


Figure 3: Results for $\ln F \equiv \ln(\Gamma/m_\phi^2 L)$ for $\xi = 4$ and volume $L' = 16$. The diagonal solid line represents the analytic semiclassical result (12). The two solid lines extending from small β into the intermediate temperature region represent high temperature fits of the form $F = c_0 + c_2 \beta^{-2}$ [9]. The upper data are for $a' = 0.32$, the lower data for $a' = 0.16$. The figure also shows at very small β a fit of $F = c_0 + c_{2/3} \beta^{-2/3}$ to the $a' = 16$ data.

0.16 the classical rate in this temperature region is lattice spacing independent, within the errors. From the perturbative analysis in sect. 3 we see no reason to doubt that the limit of zero lattice spacing exists in the weak coupling region and that the resulting ratio $\Gamma_{\text{class}}/\Gamma_{\text{semi-class}}$ approaches one as $\beta \rightarrow \infty$.

7 High temperature region

Decreasing β we see in fig. 3 that the rate is at first more or less temperature-independent, after which an apparent T^2 behavior sets in, which seems to confirm the expectation (13). However, there is substantial lattice spacing dependence in this temperature region and our earlier analysis lead to the conclusion that the coefficient c_2 in the fit $F = c_0 + c_2 T'^2$ is proportional to a'^2 , such that the rate turned out temperature-independent in the limit of zero lattice spacing [9]. Here we reconsider the situation at higher temperatures. We generated new data in the region $1.5 \leq T' \leq 5$ (input $\beta = 0.75, 0.65, 0.45, 0.29, 0.23, 0.2$), with volume $L' = 16$. At these temperatures this value of L' is amply sufficient for avoiding significant volume dependence. The lattice spacings were given by $a' \approx 0.25, 0.23, 0.16, 0.11, 0.08$ ($a' = L'/N$, $N = 63, 71, 100, 141, 200$). At first we tried extrapolating to zero lattice spacing and seeing if the resulting rate showed a T^2 or $T^{2/3}$ behavior, but in this way the errors turned out too large to allow for a meaningful discrimination between these two alternatives. We therefore looked at the temperature dependence at fixed lattice spacing, with the following amusing outcome: the larger lattice spacings $a' = 0.25, 0.23$, favor T^2 behavior while the smaller spacings $a' = 0.16, 0.11$ and 0.08 favor $T^{2/3}$ behavior. Figs. 4 and 5 show two examples (as before T' in the plots is the output temperature). Fitting the form $F = c_0 + c_2 T'^2$ (cf. (47)) led to $\chi^2/\text{d.o.f.} = 1.4, 0.42, 6.5, 4.8, 3.45$, for $a' = 0.25, 0.23, 0.16, 0.11, 0.08$, respectively, while $F = c_0 + c_{2/3} T'^{2/3}$ led to $\chi^2/\text{d.o.f.} = 28.9, 21.6, 2.5, 1.1, 1.2$. Clearly, the $T^{2/3}$ form is favored for the three smaller lattice spacings. We extrapolated the resulting $c_{2/3}$ to zero lattice spacing, assuming a quadratic dependence on a' (cf. fig. 6), with the result $c_{2/3}(a' = 0) = 0.00452(86)$, or

$$\tilde{\kappa} = 2c_{2/3} = 0.0090(17), \quad \xi = 4. \quad (49)$$

It seems reasonable that the lattice spacing dependence falls like a^2 as $a \rightarrow 0$, since the equations of motion are based on an action with $O(a^2)$ discretization

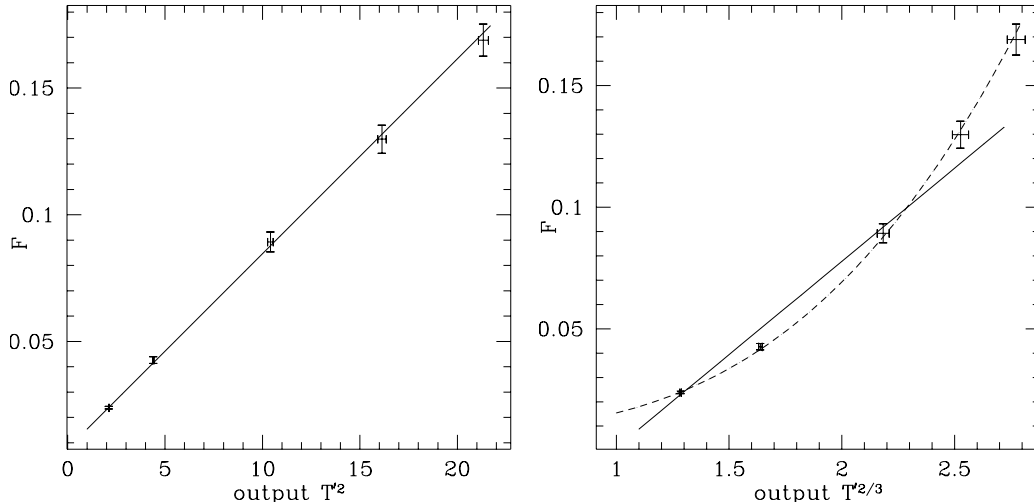


Figure 4: Data showing T^2 behavior for relatively large lattice spacing, $a' = 0.23$. Left: F versus T'^2 and a fit to $c_0 + c_2 T'^2$. Right: same data versus $T'^{2/3}$ with the T'^2 fit of the left plot (dashed line) and a fit to $c_0 + c_{2/3} T'^{2/3}$ (solid line).

errors. This could be upset by divergences, such that odd powers of a appear, as in 3+1 dimensions, but these are not expected here since we have seen in sect. 3 that the classical theory is finite.

8 Conclusion

On the basis of perturbation theory we have argued that the effectively classical approximation becomes exact in the limit (30) of weak coupling and high temperature. Furthermore, for correlation functions the classical theory is finite, which means that we can in principle obtain continuum answers by extrapolating the numerical results to zero lattice spacing. This avoids having to determine an effective action with lattice spacing dependent counterterms, as we previously deemed necessary [9]. In the limit (30) the purely classical action is sufficient to leading order.

In the resulting classical model we can still distinguish a low and high temperature regions separated by a crossover domain, as illustrated by the behavior of the rate in Fig. 3. In the low temperature region the rate is well

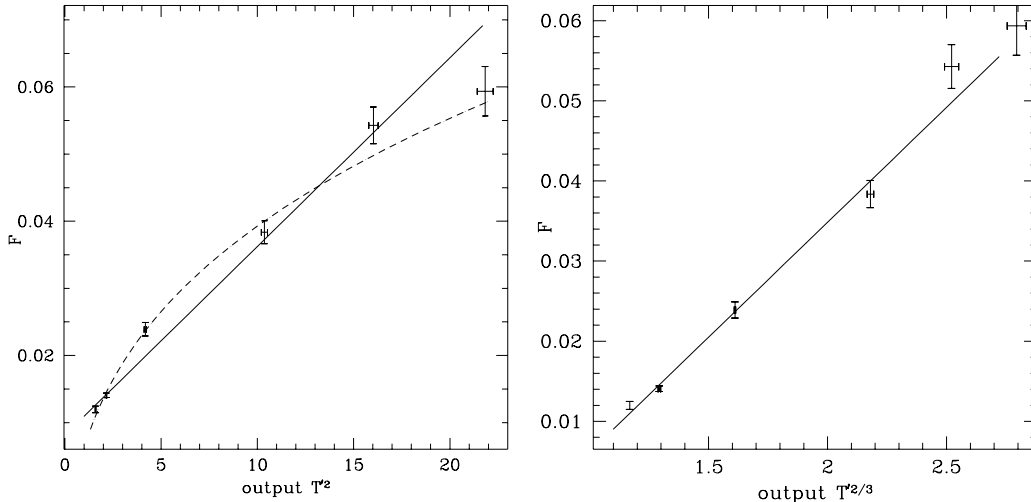


Figure 5: Data illustrating the $T^{2/3}$ behavior at small lattice spacings, $a' = 0.16$. Right: F versus $T^{2/3}$ and a fit to $c_0 + c_2 T^{2/3}$. Left: same data versus T^2 with the $T^{2/3}$ fit of the right plot (dashed line), and a fit to $c_0 + c_2 T^2$ (solid line).

described by the analytic form based on the sphaleron [10], as observed earlier [4, 7, 6]. The lattice spacing dependence is small in this region, of the order of the error bars ($\approx 10\%$). Upon crossing over to the high temperature region the lattice spacing dependence grows, and leads to a tricky phenomenon: apparently $\Gamma/L \propto T^2$ at intermediate lattice spacings, but this turns into a $T^{2/3}$ behavior in the continuum limit. We obtained the estimate $\Gamma/L = 0.0090(17)(\lambda T)^{2/3}$, $T \rightarrow \infty$, for $\xi = g^2/\lambda = 4$.

As mentioned in the Introduction, arguments for a $T^{2/3}$ behavior were previously given in ref. [8]. It was shown there that the classical rate could be written in terms of a function $g(x, y)$, as $\Gamma/L = T^{2/3} g(a^3 T, v^3/T)$, using units in which $\lambda = 1$, suppressing ξ dependence. For high temperatures $T^{2/3}$ behavior then followed in the continuum limit provided $g(0, 0) \neq 0$, ∞ existed. For the case $v^2 = 0$, numerical data supported a nontrivial $g(0, 0)$. However, for $v^2 = 1$ (which corresponds to our scaled units (36)) the results for the rate were not compared to $T^{2/3}$ behavior with much precision. The data looked compatible with our's at the time [9], but since it was taken at different ξ ($\xi = 10$) a detailed comparison was not meaningful. Our analytic

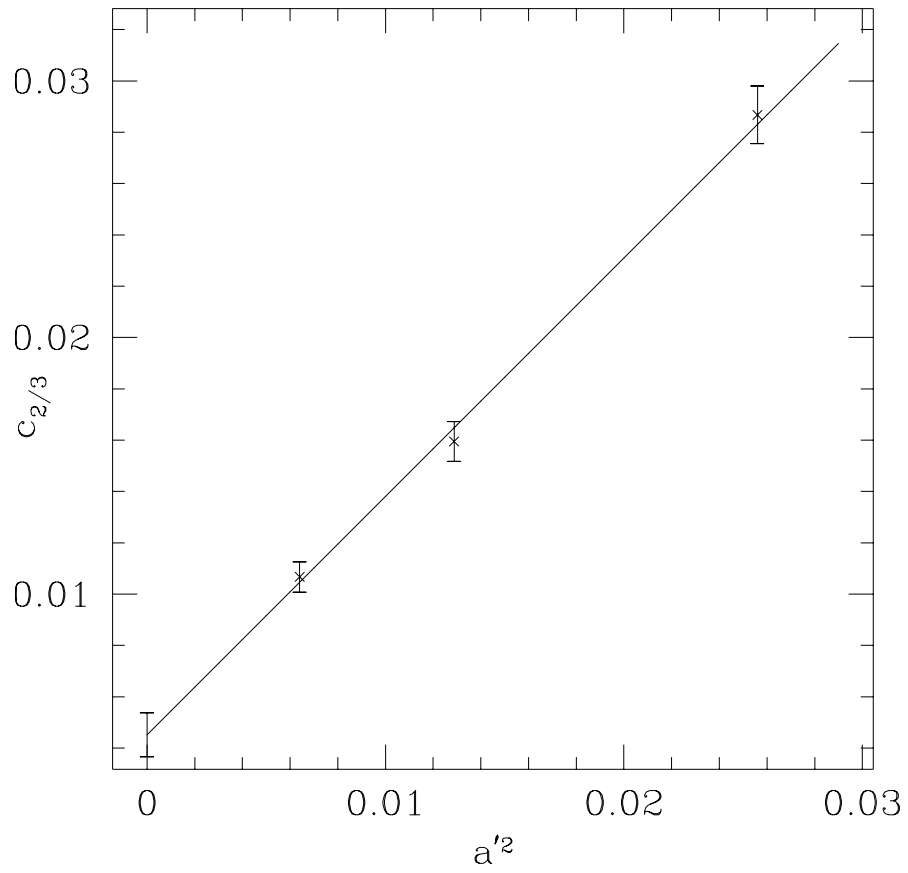


Figure 6: Plot of $c_{2/3}$ as a function of a'^2 .

results in Sect. 3 support the existence of a continuum limit of $g(a^3T, v^3/T)$, but notice how the combination a^3T implies non-commutativity of the limits $a \rightarrow 0$ and $T \rightarrow \infty$. Such non-uniform behavior complicated our numerical analysis indeed.

Acknowledgements

We like to thank A.I. Bochkarev, A. Krasnitz and G. Aarts for useful discussions. This work is supported by FOM/NWO. Numerical simulations were carried out on the CRAY C90 with financial support from NCF/NWO.

A Simulation algorithm using Kramers equation

This appendix we describe the second order Langevin algorithm, closely related to ‘Kramers equation’. Consider the class of systems described by the lagrangian

$$L = \frac{1}{2}g_{\alpha\beta}(q)\dot{q}^\alpha\dot{q}^\beta - V(q), \quad (50)$$

where $g_{\alpha\beta}$ plays the role of a metric in coordinate space. We shall assume that $g_{\alpha\beta}$ can be expressed in the form

$$g_{\alpha\beta} = e_{\alpha k}e_{\beta k}, \quad \alpha, \beta, k = 1, \dots, M, \quad (51)$$

where M is the number of q ’s or p ’s. The abelian Higgs model in polar coordinates can be described this way. It is useful to have in mind a simple two dimensional illustration given by

$$L = \dot{\phi}^*\dot{\phi} - V(\phi) \quad (52)$$

$$= \dot{\rho}^2 + \rho^2\dot{\theta}^2 - V(\rho, \theta), \quad \phi = \rho e^{i\theta}, \quad (53)$$

for which

$$e_{11} = \sqrt{2}, \quad e_{22} = \sqrt{2}\rho, \quad e_{12} = e_{21} = 0. \quad (54)$$

The hamiltonian is given by

$$H = \frac{1}{2}g^{\alpha\beta}p_\alpha p_\beta + V, \quad p_\alpha = g^{\alpha\beta}\dot{q}_\beta, \quad (55)$$

where $g^{\alpha\beta}$ is the inverse of $g_{\alpha\beta}$, $g^{\alpha\beta}g_{\beta\gamma} = \delta_\gamma^\alpha$.

Discretizing time with stepsize h , $t = nh$ ($n = 0, 1, \dots$), we can derive a leapfrog algorithm by requiring the action

$$S = \sum_n [p_{\alpha n}(q_{n+1}^\alpha - q_n^\alpha) - hH(p_n, q_n)] \quad (56)$$

to be stationary under variations of the canonical variables,

$$q_{n+1}^\alpha = q_n^\alpha + h \frac{\partial H(p_n, q_n)}{\partial p_{\alpha n}}, \quad (57)$$

$$p_{\alpha n+1} = p_{\alpha n} - h \frac{\partial H(p_{n+1}, q_{n+1})}{\partial q_{n+1}^\alpha}. \quad (58)$$

We modify these equations into second order Langevin form by adding friction and noise terms to the momentum equations,

$$\begin{aligned} p_{\alpha n+1} = & p_{\alpha n} - h \frac{\partial H(p_{n+1}, q_{n+1})}{\partial q_{n+1}^\alpha} - hF_\alpha^\beta(q_{n+1})p_{\beta n} \\ & + \sqrt{2h} N_{\alpha k}(q_{n+1})\nu_{kn}, \end{aligned} \quad (59)$$

where the ν_{kn} are normalized gaussian random numbers,

$$\langle \nu_{kn} \rangle = 0, \quad \langle \nu_{kn}\nu_{k'n'} \rangle = \delta_{kk'}\delta_{nn'}. \quad (60)$$

By a suitable choice of the random forces and friction the system may equilibrate (at large times and in the limit of zero stepsize) according to the Boltzmann distribution $\exp(-H/T)$. For this it is necessary that the Boltzmann distribution is a fixed point of the associated Fokker-Planck-type equation, which is called Kramers equation [31]. This ‘stability condition’ leads to relations between F and N , which will now be derived.

By the usual arguments one can derive the evolution equation for the probability distribution $W_t(p, q)$ at time t (‘Kramers equation’)

$$\frac{W_{t+h} - W_t}{h} = \left(-\frac{\partial H}{\partial p_\alpha} \frac{\partial}{\partial q^\alpha} + \frac{\partial H}{\partial q^\alpha} \frac{\partial}{\partial p_\alpha} \right. \quad (61)$$

$$\left. + F_\alpha^\alpha + F_\alpha^\beta p_\beta \frac{\partial}{\partial p_\alpha} + M_{\alpha\beta} \frac{\partial^2}{\partial p_\alpha \partial p_\beta} + O(h) \right) W_t, \quad (62)$$

where

$$M_{\alpha\beta} = N_{\alpha k} N_{\beta k}. \quad (63)$$

The left hand side approaches \dot{W} in the limit of zero stepsize and the first two terms on the right hand side represent the usual Liouville flow, for which $\exp(-H/T)$ is a fixed point. For the other terms $\exp(-H/T)$ is also a fixed point provided that

$$0 = F_\alpha^\alpha - F_\alpha^\beta p_\beta \frac{\partial H}{T \partial p_\alpha} + M_{\alpha\beta} \left(\frac{\partial H}{T \partial p_\alpha} \frac{\partial H}{T \partial p_\beta} - \frac{\partial^2 H}{T \partial p_\alpha \partial p_\beta} \right). \quad (64)$$

Inserting the explicit form of H and comparing powers of the momenta leads to the relations between F and N ,

$$F_\alpha^\alpha = \frac{1}{T} M_{\alpha\beta} g^{\alpha\beta}, \quad (65)$$

$$\frac{1}{2}(F_\gamma^\alpha g^{\gamma\beta} + F_\gamma^\beta g^{\gamma\alpha}) = \frac{1}{T} M_{\gamma\delta} g^{\gamma\alpha} g^{\delta\beta}. \quad (66)$$

This is satisfied by

$$F_\alpha^\beta = \frac{1}{T} M_{\alpha\gamma} g^{\gamma\beta}, \quad (67)$$

which gives F in terms of M and the metric,

Ergodicity and stability should guarantee that the evolution approaches the canonical distribution for $t \rightarrow \infty$. This can be understood intuitively by writing

$$W_t = e^{-H/2T} \tilde{W}_t. \quad (68)$$

The distribution \tilde{W}_t evolves according to

$$\frac{\tilde{W}_{t+h} - \tilde{W}_t}{h} + \left(\frac{\partial H}{\partial p_\alpha} \frac{\partial}{\partial q^\alpha} - \frac{\partial H}{\partial q^\alpha} \frac{\partial}{\partial p_\alpha} \right) \tilde{W}_t = -P \tilde{W}_t, \quad (69)$$

with

$$P = \left(-\frac{\partial}{\partial p_\alpha} + \frac{g^{\alpha\gamma} p_\gamma}{2T} \right) M_{\alpha\beta} \left(\frac{\partial}{\partial p_\beta} + \frac{g^{\beta\delta} p_\delta}{2T} \right). \quad (70)$$

The Liouville operator on the left hand side conserves probability. On the other hand, since M is evidently a positive matrix, the differential operator P is positive definite. Expanding \tilde{W}_t in terms of the eigenmodes of P , the

modes with nonzero eigenvalues are expected to die out during the time evolution, such that \tilde{W}_t approaches the zero mode $\exp(-H/2T)$,

$$\left(\frac{\partial}{\partial p_\beta} + \frac{g^{\beta\delta} p_\delta}{2T} \right) e^{-H/2T} = 0, \quad (71)$$

which is of course also a zero mode of the Liouville operator. The original W_t then approaches the Boltzmann distribution with temperature T .

A natural choice for N is given by

$$N_{\alpha k} = \sqrt{fT} e_{\alpha k}, \quad M_{\alpha\beta} = fT g_{\alpha\beta}, \quad F_\alpha^\beta = f\delta_\alpha^\beta, \quad (72)$$

with some arbitrary friction coefficient $f > 0$. However, in our application to the abelian Higgs model we want to add noise only to the radial momenta p_ρ and not to the angular momenta p_θ . Therefore, N and M contain a projector onto the radial variables,

$$N_{\alpha k} = \sqrt{fT} e_{\alpha l} \pi_{lk}, \quad \pi_{kl} \pi_{lm} = \pi_{km}, \quad (73)$$

where π is the projector. In the above two dimensional model this is illustrated by

$$\pi_{11} = 1, \quad \pi_{12} = \pi_{21} = \pi_{22} = 0, \quad (74)$$

and consequently

$$N_{11} = \sqrt{2fT}, \quad M_{11} = 2fT, \quad F_1^1 = f, \quad (75)$$

with the other components vanishing. These N and F are independent of ρ and θ .

References

- [1] A.G. Cohen, D.B. Kaplan, A.E. Nelson, Ann. Rev. Nucl. Part. Sci. 43 (1993) 27.
- [2] V.A. Rubakov and M.E. Shaposhnikov, Usp. Fiz. Nauk 166i (1996) 493, Phys. Usp. 39 (1996) 461, hep-ph/9603208.
- [3] D.Yu. Grigoriev and V.A. Rubakov, Nucl. Phys. B299 (1988) 67.

- [4] D.Yu. Grigoriev, V.A. Rubakov and M.E. Shaposhnikov, Nucl. Phys. B326 (1989) 737.
- [5] A.I. Bochkarev and Ph. de Forcrand, Phys. Rev. D44 (1991) 519.
- [6] J. Smit and W.H. Tang, Nucl. Phys. B (Proc. Suppl.) 34 (1994) 616.
- [7] A. Krasnitz and R. Potting, Nucl. Phys. B (Proc. Suppl.) 34 (1994) 613.
- [8] P. de Forcrand, A. Krasnitz and R. Potting, Phys. Rev. D50 (1994) 6054.
- [9] J. Smit and W.H. Tang, Nucl. Phys. B (Proc. Suppl.) 42 (1995) 590.
- [10] A.I. Bochkarev and G.G. Tsitsishvili, Phys. Rev. D40 (1989) 1378.
- [11] J. Ambjørn, T. Askgaard, H. Porter and M.E. Shaposhnikov, Phys. Lett. B244 (1990) 479; Nucl. Phys. B353 (1991) 346;
- [12] J. Ambjørn and A. Krasnitz, Phys. Lett. B362 (1995) 97; Nucl. Phys. B506 (1997) 387.
- [13] W.H. Tang and J. Smit, Nucl. Phys. B482 (1996) 265.
- [14] G.D. Moore and N.G. Turok, Phys. Rev. D56 (1997) 6533.
- [15] G.D. Moore, C.H. Hu and B. Müller, hep-ph/9710436.
- [16] G.D. Moore, hep-ph/9801204.
- [17] D. Bödeker, L. McLerran and A. Smilga, Phys. Rev. D52 (1995) 4675.
- [18] P. Arnold, Phys. Rev. D 55 (1997) 7781.
- [19] G. Aarts and J. Smit, Phys. Lett. B393 (1997) 395.
- [20] G. Aarts and J. Smit, Nucl. Phys. B511 (1998) 451.
- [21] W. Buchmüller and A. Jakovac, Phys. Lett. B407 (1997) 39.
- [22] W.H. Tang and J. Smit, Nucl. Phys. B510 (1998) 401.
- [23] B. Bödeker and M. Laine, hep-ph/9707489.

- [24] P. Arnold and L.G. Yaffe, *Phys. Rev. D* 57 (1998) 1178.
- [25] D. Jones, J. Kogut and D. Sinclair, *Phys. Rev. D* 10 (1979) 1882.
- [26] I. Ichinose, H. Mukaida, *Int. J. Mod. Phys. A* 9 (1994) 1043.
- [27] H. Dilger and J. Heitger, *Nucl. Phys. B (Proc. Suppl.)* 53 (1997) 587.
- [28] S.Yu. Khlebnikov and M.E. Shaposhnikov, *Nucl. Phys. B* 308 (1988) 885.
- [29] A.I. Bochkaev and M.E. Shaposhnikov, *Mod. Phys. Lett. A* 12 (1987) 991.
- [30] M. Le Bellac, *Thermal Field Theory*, CUP 1996.
- [31] N.G. van Kampen, *Stochastic Processes in Physics and Chemistry*, North-Holland 1981.